Available online at www.sciencedirect.com

SciVerse ScienceDirect

Procedia Engineering 00 (2017) 000–000

Procedia Engineering

www.elsevier.com/locate/procedia

arXiv:1706.01344v1 [cs.NA] 2 Jun 2017

DRAFT - 26th International Meshing Roundtable

Computing two dimensional cross fields A PDE approach based on the Ginzburg-Landau theory

Pierre-Alexandre Beaufort[a,b], Jonathan Lambrechts[a], François Henrotte[a,b], Christophe Geuzaine[b], Jean-François Remacle[a]

[a] *Université catholique de Louvain, iMMC, Avenue Georges Lemaitre 4, 1348 Louvain-la-Neuve, Belgium*
[b] *Université de Liège, Montefiore Institute, Allée de la Découverte 10, B-4000 Liège, Belgium*

Abstract

Cross fields are auxiliary in the generation of quadrangular meshes. A method to generate cross fields on surface manifolds is presented in this paper. Algebraic topology constraints on quadrangular meshes are first discussed. The duality between quadrangular meshes and cross fields is then outlined, and a generalization to cross fields of the Poincaré-Hopf theorem is proposed, which highlights some fundamental and important topological constraints on cross fields. A finite element formulation for the computation of cross fields is then presented, which is based on Ginzburg-Landau equations and makes use of edge-based Crouzeix-Raviart interpolation functions. It is first presented in the planar case, and then extended to a general surface manifold. Finally, application examples are solved and discussed.
© 2017 The Authors. Published by Elsevier Ltd.
Peer-review under responsibility of the organizing committee of IMR 26.

Keywords: Ginzburg-Landau theory, Cross Fields, Quadrangle meshing, Poincaré-Hopf, Crouzeix-Raviart

1. Introduction

Quadrangular elements are usually considered, in the finite element community, to be better than triangular elements, because there are twice as much triangles than quadrangles in a mesh for the same number of vertices. Moreover, quadrangular elements support tensorial operations, and ease tracking preffered directions in mesh refinement. Producing high quality quadrangular meshes is however not a trivial task. An appropiate approach [1] is the *indirect* one. It consists of (i) spawning points, (ii) triangulate them, and finally (iii) recombine triangles into quadrangles.

Even if the two last steps are performed by efficient algorithms [2], the final mesh quality strongly depends on the adequacy of the position of the spawned points with a potential quadrangular grid. A way to position points adequately in view of generating a mesh with quadrangular elements only is to rely on a precomputed *cross field*. There exist several methods to produce cross fields, either by an optimization process [3], or by

E-mail address: jean-francois.remacle@uclouvain.be (Jean-François Remacle).

1877-7058 © 2017 The Authors. Published by Elsevier Ltd.
Peer-review under responsibility of the organizing committee of IMR 26.

solving a PDE [4]. Quality criteria for cross fields are smoothness, topology consistency, and alignment with boundaries and/or with geometrical features of the surface manifold like curvature. The partial differential cross field problem is formulated in variational form by the *Ginzburg-Landau* functional. This functional consists of a *smoothness* term that minimizes the gradient of the cross field and a *penalty* term that ensures its norm remains closed to unity. The Ginzburg-Landau formulation naturally gives fields with minimum *critical points* of minimum index. *Crouzeix-Raviart finite elements* are used for the interpolation and the nonlinear problem is solved using a *Newton-Raphson scheme.*

2. Topology of triangular and quadrilateral meshes

Assume an orientable surface $\mathcal{S}$ embedded in $\mathbb{R}^3$. Let g be the number of handles of the surface. The topological characteristic g, which is also called the genus of the surface, is the maximum number of cuttings along non-intersecting closed curves that won't make the surface disconnected. Let also b be the number of connected components of the boundary $\partial\mathcal{S}$ of the surface. The Euler characteristic of $\mathcal{S}$ is then the integer

$$\chi = 2 - 2g - b. \tag{1}$$

One has $\chi = 2$ for a sphere, whereas $\chi = 1$ for a disk ($b = 1$), and $\chi = 0$ for a torus ($g = 1$) or a cylinder ($b = 2$).

Consider now a mesh on $\mathcal{S}$ with n nodes (also called vertices), n_e edges and n_f facets. The Euler formula

$$\chi = n - n_e + n_f$$

provides a general relationship betweeen the numbers of nodes, edges and facets in the mesh [5]. If n_b nodes (and hence n_b edges) are on the boundary $\partial\mathcal{S}$, and if the number of edges (or nodes) per facet is noted n_{evf} ($n_{evf} = 3$ for triangulations and $n_{evf} = 4$ for quadrangulations, meshes mixing triangles with quadrangles being excluded), the following identity holds: all facets have n_{evf} edges, $n_e - n_b$ edges have two adjacent facets and n_b edges have one adjacent facet. Hence the relationship

$$n_{evf} n_f = 2(n_e - n_b) + n_b. \tag{2}$$

Elimination of n_e between (2) and (1) yields

$$2n - n_b + (2 - n_{evf})n_f = 2\chi, \tag{3}$$

which is true for any triangulation or quadrangulation.

A regular mesh has only regular vertices. An internal vertex is regular if it has exactly 6 adjacent triangles or 4 adjacent quadrangles, whereas a boundary vertex is regular if it has exactly 3 adjacent triangles or 2 adjacent quadrangles. One has then

$$6(n - n_b) + 3n_b = 3n_f \quad \Rightarrow \quad n_f = 2n - n_b \tag{4}$$

and

$$4(n - n_b) + 2n_b = 4n_f \quad \Rightarrow \quad n_f = n - \frac{n_b}{2} \tag{5}$$

respectively for a regular triangulation and a regular quadrangulation. Substitution of (4) and (5) into (3) shows that only surfaces with a zero Euler characteristic can be paved with a regular mesh. If $\chi \neq 0$, irregular vertices will necessarily be present in the mesh.

The number and the index of the irregular vertices is tightly linked to the Euler characteristic χ, which is a topological invariant of the surface. We call valence of a vertex the number of facets adjacents to the vertex in the mesh. In a regular mesh, all vertices have the same valence v_{reg}. In a non regular mesh, on the other hand, a number of irregular vertices have a valence $v \neq v_{reg}$, and one notes the integer $k = v_{reg} - v$ the valence mismatch of a vertex.

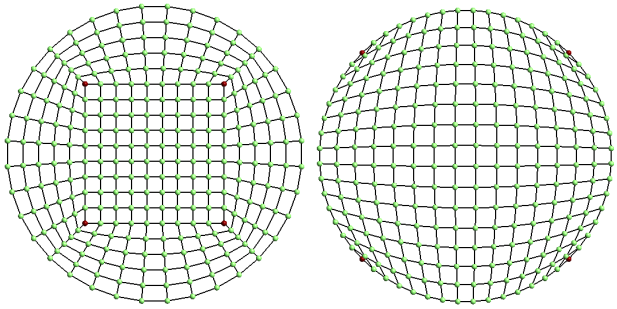

Figure 1: A quadrilateral mesh of a circle. Four irregular vertices of index 1/4 (in red) are required to obtain such a mesh. The irregular vertices may be inside the disk (left) or on its boundary (right)

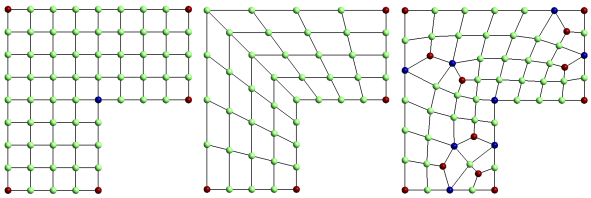

Figure 2: Different quadrangulations of a L-shaped domain. Irregular vertices of index 1 are displayed in red, whereas ones of index −1/4 are displayed in blue. The sum of the indices of the irregular vertices is equal to $\chi = 1$ in all cases.

Assume a quadrangulation with n_k irregular internal vertices of valence $v = 4 - k$, and n_{bk} irregular boundary vertices of valence $2 - k$, k given. All other vertices are regular. There are then $n - n_b - n_k$ regular internal vertices of valence 4, and $n_b - n_{bk}$ regular boundary vertices of valence 2, so that one can write

$$4n_f = 4(n - n_b - n_k) + 2(n_b - n_{bk}) + (4 - k)n_k + (2 - k)n_{bk}, \tag{6}$$

and the substraction of (3) with $n_{evf} = 4$ yields

$$\chi = \frac{k}{4}(n_k + n_{bk}),$$

showing that, in a quadrangulation, each irregular vertex counts for $\text{index}(\mathbf{x}_i) = k/4$ in the Euler characteristic, a quantity called the indice of the irregular vertex $\mathbf{x}_i$.

Summing up now on different possible values for k, one can establish that a quadrangulation of a surface with Euler characteristic χ verifies

$$\chi = \sum_k \frac{k}{4}(n_k + n_{bk}) = \sum_{i=1}^{N} \text{index}(\mathbf{x}_i). \tag{7}$$

Consider, for instance, the quadrangulation of a disk, which is a surface with $\chi = 1$. A minimum of $n_1 = 4$ irregular vertices of index 1/4 must be present. They can be located either on the boundary (vertices of valence 1) or inside the disk (vertices of valence 3), Figure 1.

Figure 2 shows three different quadangulations of a L-shaped domain ($\chi = 1$). Regular boundary nodes should all have a valence of 2. The mesh on the left has 6 irregular vertices located at the corners of the domain : five with index 1/4, and one with index −1/4. The central mesh, on the other hand, has the minimum amount of irregular vertices, i.e., four ones of index 1/4. The right mesh generated by recombination of a standard Delaunay triangular mesh [2] has eight vertices of index 1/4, and twelve vertices of index −1/4, both on the boundary and inside the domain. Quality meshes should have as few irregular vertices as possible. In what follows, a general method allowing to position irregular vertices before meshing the surface is presented.

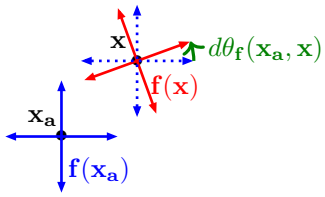

Figure 3: Diffential function $\mathrm{d}\theta_f$.

3. Why cross fields ?

Cross fields are auxiliary in the generation of quadrangular meshes. We shall show that nonregular vertices defined in the previous section are precisely the critical points of a cross field, and that these critical points of the cross field can also be related to the Euler characteristic of the meshed surface. This result represents an important theoretical limit on the regularity of quadrangular meshes.

3.1. Continuity

A cross field f is a field defined on a surface $\mathcal{S}$ with values in the quotient space S^1/Q, where S^1 is the circle group and Q is the group of quadrilateral symmetry. Pictorially, it associates to each point of the surface $\mathcal{S}$ to be meshed a cross made of four unit vectors orthogonal with each other in the tangent plane $T\mathcal{S}$ of the surface.

A surface $\mathcal{S}$ can be identified with its tangent space in any neighborhood $\sigma \subset \mathcal{S}$ that is sufficiently small to have curvature effects negligible. This local identification of the surface with a vector space endows it with a natural parallel transport rule, so that the angular differential $\mathrm{d}\theta_f(\mathbf{x}_a, \mathbf{x}_b)$ can be defined as the minimal angle, with its sign, between the branches of $f(\mathbf{x}_a)$ and any of the branches of $f(\mathbf{x}_b)$ for any pair of points $\mathbf{x}_a, \mathbf{x}_b \in \sigma$ where f is defined, Fig. 3. Taking now as reference the cross $f(\mathbf{x}_a)$, an angular coordinate

$$\theta_f(\mathbf{x}) = \mathrm{d}\theta_f(\mathbf{x}_a, \mathbf{x}) \tag{8}$$

can be defined for crosses in σ. The cross field f is deemed continuous (regular) in $\mathbf{x}_b$ if the limit

$$\lim_{\mathbf{x}\to\mathbf{x}_b} \theta_f(\mathbf{x}) = \theta_f(\mathbf{x}_b) \tag{9}$$

exists (i.e., is unique). It is then equal to $\theta_f(\mathbf{x}_b)$. Isolated points $\mathbf{x}_i,\ i = 1 \ldots N$, of $\mathcal{S}$ where the limit (9) does not exist are called critical points or zeros of the cross field.

3.2. Index and degree

Although defined locally, the notion of continuity gives unexepectedly valuable information about the topology of $\mathcal{S}$, which is a nonlocal concept. To see this, consider a cross field f defined on a quandrangular element delimited by four (possibly curvilinear) edges. Assume the cross field is parallel to the four edges (i.e., one of the four branches of the cross is parallel to the tangent vector of the edge at each point of the edge, except the extremities) and prolongates smoothly inside the quadrangle. This field is discontinuous at corners where edges do not meet at right angle, but it is continous everywhere else. Making the same construction for all elements of a quadrangular mesh, one obtains a cross field f topologically identified with the quadrangular mesh, and that is continuous everywhere except at the vertices of the mesh. This field has thus got isolated critical points at mesh vertices, but not all critical points have the same significance. Some critical points have a specific topological value, associated with the notion of index.

To introduce the notion of index, an angular coordinate needs to be defined for points in a neighborhood σ_i of a critical point $\mathbf{x}_i$. Picking up an arbitrary regular point $\mathbf{x}_a \in \sigma_i$, $\mathbf{x}_a \neq \mathbf{x}_i$, the local unit vector basis

$$\mathbf{e}_1 = \frac{\mathbf{x}_a - \mathbf{x}_i}{|\mathbf{x}_a - \mathbf{x}_i|} \quad , \quad \mathbf{e}_2 = \mathbf{n} \times \mathbf{e}_1,$$

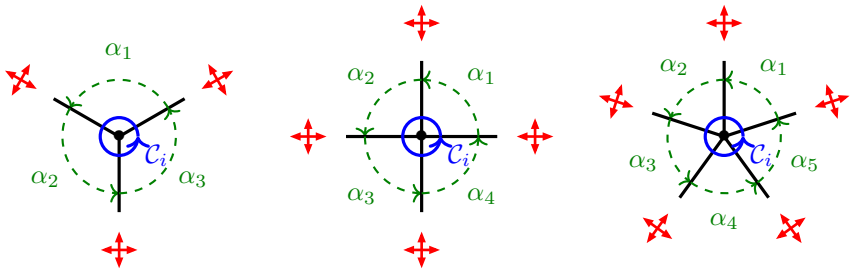

Figure 4: Illustration of vertices where the indices of the cross field represented in red are respectively $1/4, 0$ and $-1/4$, from left to right. The index only depends on the number of quadrangles adjacent to the vertex, independently of the values of the angles α_p, which need not be identical as they are in the figure.

with $\mathbf{n}$ the normal to $\mathcal{S}$, is constructed, and hence a local polar coordinate system

$$r(\mathbf{x}) = |\mathbf{x} - \mathbf{x}_i| \quad , \quad \theta(\mathbf{x}) = \operatorname{atan2}\Big((\mathbf{x} - \mathbf{x}_i) \cdot \mathbf{e}_2, (\mathbf{x} - \mathbf{x}_i) \cdot \mathbf{e}_1\Big) \tag{10}$$

can be defined for points in σ_i.

A circular curve C_i of infinitesimal radius centered around the vertex $\mathbf{x}_i$ is now considered. As the angles $\theta(\mathbf{x})$ (10) and $\theta_f(\mathbf{x})$ (8) are precisely the elements of the groups S^1 and S^1/Q, respectively, the cross field on C_i can be regarded as a mapping

$$f \, : S^1 \mapsto S^1/Q. \tag{11}$$

The mapping is continuous, since C_i circles around the critical point $\mathbf{x}_i$, but does not cross it. The index of f at $\mathbf{x}_i$ is the degree of the mapping (11), i.e., the number of times the codomain wraps around the domain under the mapping. Its algebraic expression is easily expressed in terms of the angles θ and θ_f as

$$\operatorname{index}(\mathbf{x}_i) = \frac{1}{2\pi} \oint_{C_i} \mathrm{d}\theta_f$$

where 2π is $\oint_{C_i} \mathrm{d}\theta$. In case of a vertex $\mathbf{x}_i$ of valence v_i, i.e., a vertex adjacent to v_i quandrangular elements, the integral evaluates as

$$\operatorname{index}(\mathbf{x}_i) = \frac{1}{2\pi} \sum_{p=1}^{v_i} \left(\alpha_p - \frac{\pi}{2}\right) = \frac{1}{2\pi}(2\pi - v_i \frac{\pi}{2}) = \frac{4 - v_i}{4}, \tag{12}$$

where the α_p's are the angles of the v_i quadrangular elements adjacent to the considered vertex $\mathbf{x}_i$, and where the obvious relationship $\sum_{p=1}^{v_i} \alpha_p = 2\pi$ has been used. The cross field f has index 0 at vertices adjacent to four quadrangular elements, whereas it has index $1/4$, resp. $-1/4$ at vertices adjacent to 3, resp. 5, quadrangular elements meet, Fig. 4. As one sees, the index is a topological characteristic of the cross field f at the critical point $\mathbf{x}_i$. It does not depend on the choice of the curve C_i, nor on the choice of an angular reference for the angles $\theta(\mathbf{x})$ and $\theta_f(\mathbf{x})$.

3.3. Poincaré-Hopf theorem

Equation (12), relates the index of the cross field at a critical point $\mathbf{x}_i$ with one forth of valence $k_i = 4 - v_i$ of the corresponding mesh vertex. This result can be combined with the algebraic topology result of previous section (7) that each internal irregular vertex of valence k_i counts for $k_i/4$ in the Euler characteristic of the underlying surface. This yields the relationship

$$\sum_{i=1}^{N} \operatorname{index}(\mathbf{x}_i) = \chi \tag{13}$$

for the critical points of a crossfield f defined on a surface $\mathcal{S}$.

This is a generalization Poincaré-Hopf theorem, which states that the sum of the indices of the critical points of a *vector* field $\mathbf{v}$ defined on a surface $\mathcal{S}$ without boundary is equal to the Euler characteristic of the surface. This famous theorem draws an unexpected and profound link between two apparently distinct areas of mathematics, topology and analysis. Whereas vector fields have integer indices at critical points, cross fields have indices that are multiples of 1/4. Still the topological relationship (13) of Poincaré-Hopf holds in both cases. Actually, our developments reach same inferences than [6].

4. Cross field computation : the planar case

4.1. Vector representation of cross fields

Only scalar quantities can be compared at different points of a manifold. For the comparison or, more generally, for differential calculus with nonscalar quantities like cross fields, a parallel transport rule needs to be defined on the manifold. On a surface manifold, this rule can take the form of a regular vector field which gives at each point the direction of the reference angle 0. Poincaré-Hopf theorem says that such a field does not exist in general, and in particular on manifolds whose Euler characteristic is not zero. The situation is however easier in the planar case. A global Cartesian coordinate frame can always be defined over the plane, and be used to evaluate the orientation of the cross field. We shall therefore expose the cross field computation method in the planar case first, and generalize to nonplanar surfaces, where we will have to deal with local reference frames, in a subsequent section.

A cross $f(\mathbf{x})$ is an element of the group S^1/Q, which can be represented by the angle $\theta_f(\mathbf{x})$ it forms with the local reference frame. Yet, due to the quadrilateral symmetry, four different angles in $[0, 2\pi[$ represent the same cross field $f(\mathbf{x})$. Let for instance the angles $\theta_1 = 0$ and $\theta_2 = \pi/2$ represent the same cross. The average $(\theta_1 + \theta_2)/2 = \pi/4$ represents another cross, whereas the difference $\theta_2 - \theta_1 = \pi/2$ is not zero. So, we have $\frac{1}{2}(x + x) \neq x$ and $x - x \neq 0$, which clearly indicates that the values of the cross field f do not live in a linear (affine) space. This makes the representation by θ_f improper for finite element interpolation. The solution is two-fold. First, the angle θ_f is multiplied by four, so that the group S^1/Q be mapped on the unit circle S^1, and the cross f be therefore represented by a unit norm vector $\mathbf{f}$. Then, the vector is represented in components in the reference frame as

$$\mathbf{f} = (\cos 4\theta_f, \sin 4\theta_f) \equiv (f_1, f_2).$$

4.2. Laplacian smoothing

Computing the cross field f consists thus now of computing the vector field representation $\mathbf{f}$, which obviously lives in a linear space (a 2D plane). The components of $\mathbf{f}$ are fixed on the boundaries of $\Gamma = \partial\mathcal{S}$ so that the crosses are parallel with the exterior normal vector $\mathbf{n} = (\cos\theta_n, \sin\theta_n)$ i.e.,

$$\mathbf{f} = (\cos 4\theta_n, \sin 4\theta_n) \quad \text{on } \Gamma.$$

Propagating $\mathbf{f}$ inside $\mathcal{S}$ is here be done by solving a Laplacian problem. Even though the vector representation $\mathbf{f}$ is unitary on Γ, it tends to drift away from S^1 inside the domain. The computed finite element solution $\mathbf{f}$ lies therefore outside the unit circle and must be projected back on S^1 to recover the angle

$$\theta_f = \frac{\operatorname{atan2}(f_2, f_1)}{4}.$$

Due to the multiplication by 4, the indices of the critical points of the vector field $\mathbf{f}$ verify

$$\sum_{i=1}^{N} \operatorname{index}(\mathbf{x}_i) = 4\chi. \tag{14}$$

4.3. The Ginzburg-Landau model

Numerical experiments show that the norm of the vector field $\mathbf{f}$ computed by Laplacian smoothing (See previous section) decreases quite rapidly as one moves away from the boundary Γ, leaving in practice large zones in the bulk of the computation domain where the solution is small, and the computed cross field inaccurate. A more satisfactory formulation consists of ensuring that the norm of $\mathbf{f}$ remains unitary over the whole computation domain. This problem can be formulated in variational form in terms of the Ginzburg-Landau functional

$$E(f_1, f_2) = \underbrace{\frac{1}{2}\int_{\mathcal{S}} \left(|\nabla f_1|^2 + |\nabla f_2|^2\right) d\mathcal{S}}_{\text{smoothing}} + \underbrace{\frac{1}{4\epsilon^2}\int_{\mathcal{S}} \left(f_1^2 + f_2^2 - 1\right)^2 d\mathcal{S}}_{\text{penality}}. \tag{15}$$

The first term minimizes the gradient of the cross field and is therefore responsible for the laplacian smoothing introduced in the previous section. The second term is a penality term that vanishes when $\mathbf{f} \in S^1$. The penality parameter ϵ, called *coherence length*, has the dimension of a length. The Euler-Lagrange equations of the functional (17) are the quasi-linear PDE's

$$\nabla^2 f_i - \frac{1}{\epsilon^2}\left(f_1^2 + f_2^2 - 1\right) f_i = 0 \quad i = 1, 2. \tag{16}$$

called Ginzburg-Landau equations. If ϵ is small (enough) with respect to the dimension of $\mathcal{S}$, then $\mathbf{f}$ is of norm 1 everywhere but in the vicinity of the isolated critical points $\mathbf{x}_i$.

The asymptotic behavior of Ginzburg-Landau energy can be written as

$$E = \pi\left(\sum_{i=1}^{N} \text{index}(\mathbf{x}_i)^2\right)\log(1/\epsilon) + W + O(1/|\log\epsilon|). \tag{17}$$

with

$$W = -\pi \sum_{i=1}^{N}\sum_{\substack{j=1\\ j\neq i}}^{N} \text{index}(\mathbf{x}_i)\ \text{index}(\mathbf{x}_j)\log|\mathbf{x}_i - \mathbf{x}_j| + R \tag{18}$$

as $\epsilon \to 0$ (see [7], Introduction, Formulae 11 and 12).

In asymptotic regime, the energy is thus composed of three terms. The first term of (17) blows up as $\epsilon \to 0$, i.e., energy becomes unbounded if critical points are present. When ϵ is small, this first term dominates, and one is essentially minimizing $\sum_{i=1}^{N} \text{index}(\mathbf{x}_i)^2$ with the constraint (14). This indicates that a critical point of index 2 has a cost of 4 in terms of energy, whereas 2 critical points of index 1 have a cost of 2. All critical points should therefore be of index ± 1, and their number should be $N = 4\,|\chi|$. This is indeed good news for our purpose: good cross fields should have few critical points of lower indices.

The second term of (17) is the *renormalized energy* W (18). It remains bounded when ϵ tends to 0. The double sum in W reveals the existence of a logarithmic force between critical points. The force is attractive between critical points with indices of opposite signs, and a repulsive between critical points with indices of the same signs. The second term in (18) is more complicated and is detailed in [7]. Basically, R represents a repulsing force that forbids critical points to approach the boundaries.

Finally, the third term in (17) vanishes as $\epsilon \to 0$. At the limit, all energy is thus carried by the critical points of the field. All this together allows to believe that Ginzburg-Landau model is a good choice for computing cross fields. It produces few critical points, which are moreover well-distributed over the domain.

5. Computation of cross fields: nonplanar generalization

The finite element computation method for cross fields is now generalized to the case of nonplanar surfaces. Consider the conformal triangulation $\mathcal{S} = \cup_{ijk}\Omega_{ijk}$ of a nonplanar surface manifold $\mathcal{S}$, each triangle Ω_{ijk} being defined by the vertices $\mathbf{p}_i$, $\mathbf{p}_j$ and $\mathbf{p}_k$. Since no global reference frame exists on a nonplanar surface, a local

reference frame is associated to each edge of the triangulation. Let e^p be the pth edge of the mesh, joining nodes $\mathbf{p}_i$ and $\mathbf{p}_j$, and $\mathbf{n}^p$ be the average of the normals vectors of the two triangles adjacent to e^p. The vectors

$$\left\{\mathbf{e}^p = \mathbf{p}_j - \mathbf{p}_i, \mathbf{t}^p = \mathbf{n}^p \times \mathbf{e}^p\right\}$$

form a local frame $\{\hat{e}^p, \hat{t}^p\}$ in which to represent the connector values of the discretized cross field $\mathbf{f}$,

$$f_1^p = \cos 4\theta_f^p \quad , \quad f_2^p = \sin 4\theta_f^p,$$

which are attached to the center of the edges of the triangulation. Actually, θ_f^p is assumed to be the same along $\boldsymbol{e}^p$ within both planes of triangles sharing e^p. This assumption eases computation and gives a planar-like representation, Fig. 5a.

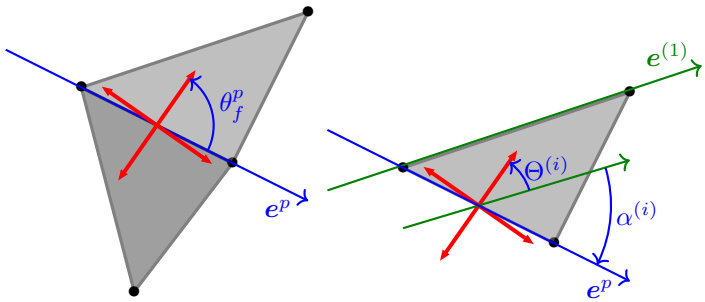

a. Global representation. b. Local representation.

Figure 5: Cross field within a triangulation.

As the connector values are attached to the edges of the mesh, and not to the nodes, Crouzeix-Raviart interpolation functions are used instead of conventional Lagrange shape functions [8]. The Crouzeix-Raviart shape functions ω^p equal 1 on corresponding edge e^p, and -1 on the opposite vertices (Fig. 6) in the two adjacent triangular elements. They are polynomial and their analytic expression in the reference triangle $\{\xi \in [0,1], \quad \eta \in [0, 1-\xi]\}$ reads

$$\omega^{(1)}(\xi,\eta) = 1 - 2\eta \quad , \quad \omega^{(2)}(\xi,\eta) = 2(\xi+\eta) - 1 \quad , \quad \omega^{(3)}(\xi,\eta) = 1 - 2\xi,$$

where indices (1), (2) and (3) enclosed in parenthesis denote the local edge numbering in the considered triangular element.

Each of the three edges of a triangle Ω_{ijk} has its own local reference frame. If one is to interpolate expressions involving the vector field $\mathbf{f}$ over this element, the three edge-based reference frames have to be appropriately related with each other [9]. We arbitrarily take the reference frame of the first edge of the element as reference, and express the angular coordinate of the two other edges in function of this one with the relationships (Fig. 5b)

$$\Theta^{(1)} = \theta_f^{(1)} \quad , \quad \Theta^{(2)} = \theta_f^{(2)} + \alpha^{(2)} \quad , \quad \Theta^{(3)} = \theta_f^{(3)} + \alpha^{(3)}.$$

Thus, the 6 local unknowns of triangle Ω_{ijk} can be expressed as a function of the 6 edge unknowns by

$$\begin{pmatrix} \cos 4\Theta^{(1)} \\ \cos 4\Theta^{(2)} \\ \cos 4\Theta^{(3)} \\ \sin 4\Theta^{(1)} \\ \sin 4\Theta^{(2)} \\ \sin 4\Theta^{(3)} \end{pmatrix} \equiv \underbrace{\begin{pmatrix} F_1^{(1)} \\ F_1^{(2)} \\ F_1^{(3)} \\ F_2^{(1)} \\ F_2^{(2)} \\ F_2^{(3)} \end{pmatrix}}_{\mathbf{F}^{ijk}} = \underbrace{\begin{bmatrix} 1 & 0 & 0 & 0 & 0 & 0 \\ 0 & \cos 4\alpha^{(2)} & 0 & 0 & \sin 4\alpha^{(2)} & 0 \\ 0 & 0 & \cos 4\alpha^{(3)} & 0 & 0 & \sin 4\alpha^{(3)} \\ 0 & 0 & 0 & 1 & 0 & 0 \\ 0 & -\sin 4\alpha^{(2)} & 0 & 0 & \cos 4\alpha^{(2)} & 0 \\ 0 & 0 & -\sin 4\alpha^{(3)} & 0 & 0 & \cos 4\alpha^{(3)} \end{bmatrix}}_{\mathbf{R}^{ijk}} \underbrace{\begin{pmatrix} f_1^{(1)} \\ f_1^{(2)} \\ f_1^{(3)} \\ f_2^{(1)} \\ f_2^{(2)} \\ f_2^{(3)} \end{pmatrix}}_{\mathbf{f}^{ijk}}$$

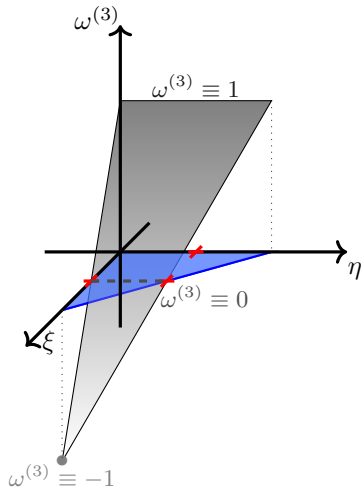

Figure 6: Third Crouzeix-Raviart function shape (shaded in grey) over reference triangle (in blue).

and we have the interpolation

$$F_1^{ijk}(\xi,\eta) = \sum_{i=1}^{3} \omega^{(i)}(\xi,\eta)\ F_1^{(i)} \quad , \quad F_2^{ijk}(\xi,\eta) = \sum_{i=1}^{3} \omega^{(i)}(\xi,\eta)\ F_2^{(i)}$$

for the vector field $\mathbf{f}$ in the triangle Ω_{ijk}.

A Newton scheme is proposed to converge to the solution. The Newton iteration at stage n for solving (16) consists of solving:

$$\nabla^2 \begin{pmatrix} f_1 \\ f_2 \end{pmatrix}_n + \frac{1}{\epsilon^2} \begin{pmatrix} 3f_1^2 & 2f_1f_2 \\ 2f_1f_2 & 3f_2^2 \end{pmatrix}_{n-1} \begin{pmatrix} f_1 \\ f_2 \end{pmatrix}_n = -\frac{1}{\epsilon^2} \begin{pmatrix} 1-4f_1^3-3f_1f_2^2 \\ 1-3f_1^2f_2-4f_2^3 \end{pmatrix}_{n-1} \tag{19}$$

The 6×6 elementary matrix $\mathbf{K}^{ijk}$ and the 6×1 elementary vector $\mathbf{B}^{ijk}$ of element Ω_{ijk} evaluate then as

$$\mathbf{K}^{ijk} = \begin{bmatrix} \left(\int_{\Omega_{ikj}} \nabla\omega_m \cdot \nabla\omega_n + \frac{3}{\epsilon^2}F_1^2\omega_m\omega_n\ d\Omega\right)_{m,n=1\ldots3} & \left(\int_{\Omega_{ijk}} \frac{2}{\epsilon^2}F_1F_2\omega_m\omega_n\ d\Omega\right)_{m,n=1\ldots3} \\ \left(\int_{\Omega_{ijk}} \frac{2}{\epsilon^2}F_1F_2\omega_m\omega_n\ d\Omega\right)_{m,n=1\ldots3} & \left(\int_{\Omega_{ikj}} \nabla\omega_m \cdot \nabla\omega_n + \frac{3}{\epsilon^2}F_2^2\omega_m\omega_n\ d\Omega\right)_{m,n=1\ldots3} \end{bmatrix} \tag{20}$$

and

$$\mathbf{B}^{ijk} = \frac{1}{\epsilon^2} \begin{pmatrix} \left(\int_{\Omega_{ijk}} (1-4F_1^3-3F_1F_2^2)\omega_n\ d\Omega\right)_{n=1\ldots3} \\ \left(\int_{\Omega_{ijk}} (1-3F_1^2f_2-4F_2^3)\omega_n\ d\Omega\right)_{n=1\ldots3} \end{pmatrix}. \tag{21}$$

It is then necessary to transform those elementary matrix and vector in the reference frames of the edges as

$$\mathbf{k}^{ijk} = (\mathbf{R}^{ijk})^T\mathbf{K}^{ijk}\mathbf{R}^{ijk} \quad \text{and} \quad \mathbf{b}^{ijk} = (\mathbf{R}^{ijk})^T\mathbf{B}^{ijk}.$$

Then, standard finite element assembly can be performed. Boundary conditions are simply

$$f_1^p = 1 \quad , \quad f_2^p = 0$$

on every edge e^p of $\partial\Omega$. This nice simplification is due to the fact that unknowns are defined on the reference frame of the edges.

6. Results

6.1. The sphere

As a first example, let us compute the cross field on a unit sphere. The sphere has no boundary so we choose randomly one edge of the mesh and fix the cross field for this specific edge. The mesh of the sphere is made of 2960 triangles (see Figure 7). A value of $\epsilon = 0.1$ was chosen for the computation, which corresponds roughly to twice of the mesh size. A total of 29 Newton iterations were necessary to converge to reduce the residual by 10^{-12}. The location of the 8 critical points is indeed not what we expected: our

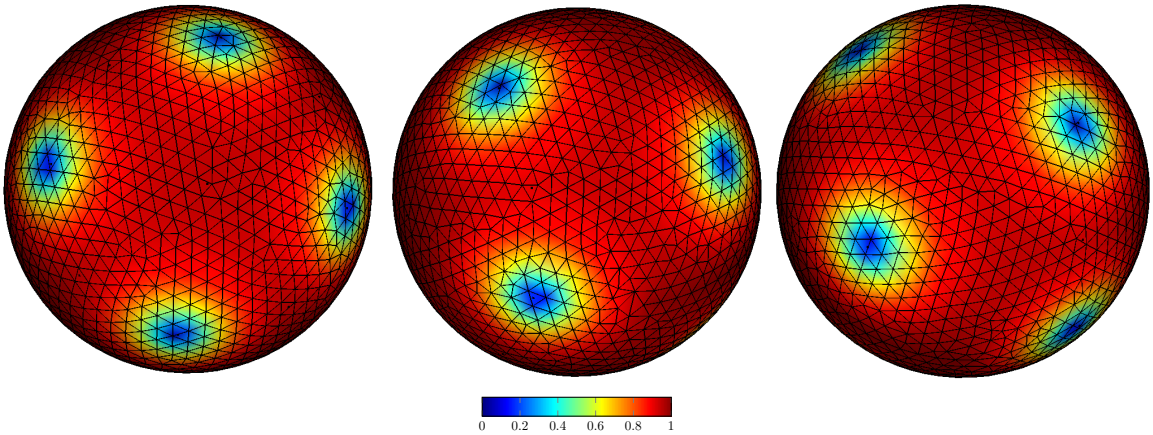

Figure 7: Mesh of the sphere. Colors correspond to the 2-norm $\|\mathbf{f}\|$ of the cross field. The 8 critical points are located on two squares of side $1/\sqrt{3}$ which correspond to the size of the inscribed cube. The two squares are tilted by 45 degrees.

initial intuition was that critical points would be located at the corners of an inscribed cube of side $1/\sqrt{3}$. In all our computations i.e. while changing the mesh and ϵ, critical points are located on two squares of side $1/\sqrt{3}$, those two squares being tilded by 45 degrees around their common axe (see Figure 7). Equilateral triangle patterns are formed between critical points that belong to both squares. In reality, our solution is the right solution. In the asymptotic regime, the location $\mathbf{x}_i$ of the 8 critical points tends to minimize $-\sum_i \sum_{i\neq j} \log|\mathbf{x}_i - \mathbf{x}_j|$ (see Equations (17) and (18)). We have thus computed $-\sum_i \sum_{i\neq j} \log|\mathbf{x}_i - \mathbf{x}_j|$ for tilting angles ranging from 0 to $\pi/2$. Figure 8 shows clearly that the minimum of the energy corresponds to an angle of $\pi/4$, which is exactly what is found by the finite element formulation. Figure 9 shows the cross field as well as the separatrices. The separatrices were computed "by hand". The solution that has been found is related to what is called the Whyte's problem [10,11] that consists of finding N points on the sphere which positions maximizes the product of their distances. The critical points are called *logarithmic extreme points* or *elliptic Fekete points* [12].

The specific configuration that corresponds to $N = 8$ is called an anticube (or square antiprism) and is exactly the one that was found numerically.

At this point, one could wonder what happens if the symmetry group of the hexagon H was used instead of the symmetry group of the square Q in the definition of the cross field. Pictorially, the cross field is then an "asterisk" field. In this case, we expect to find 12 critical points distributed in such a way that Ginzburg-Landau energy is minimized. Changing the group of symmetry simply amounts in our code in changing the rotation matrix $\mathbf{R}_{ijk}$. The results for the spherical surface are depicted in Fig. 10. Critical points are the summits of an icosahedron, which is the solution of Whyte's problem for $N = 12$. This superb result shows that it is indeed possible to use cross fields not only for building quadrangles but also to build equilateral triangles.

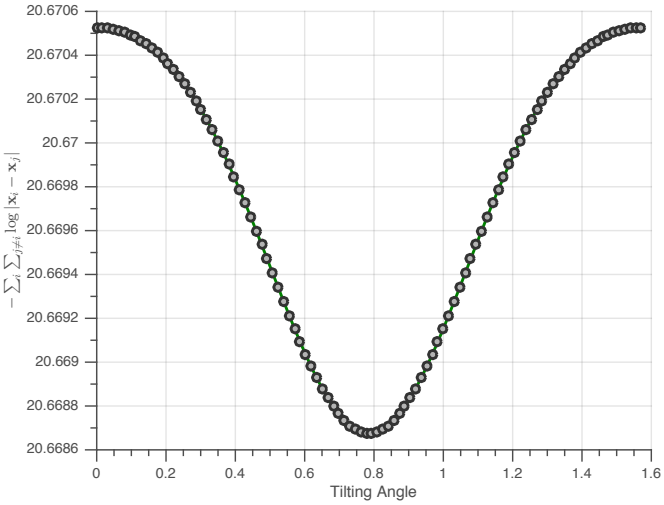

Figure 8: Energy vs. tilting angle for the sphere. The minimum corresponds to a titing angle of $\pi/4$.

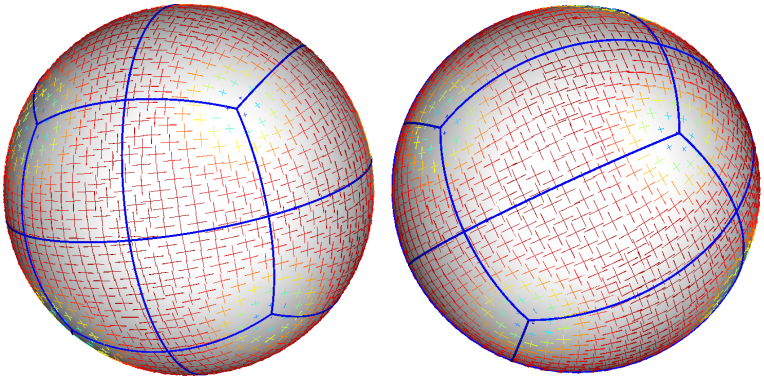

Figure 9: Cross field and separatrices.

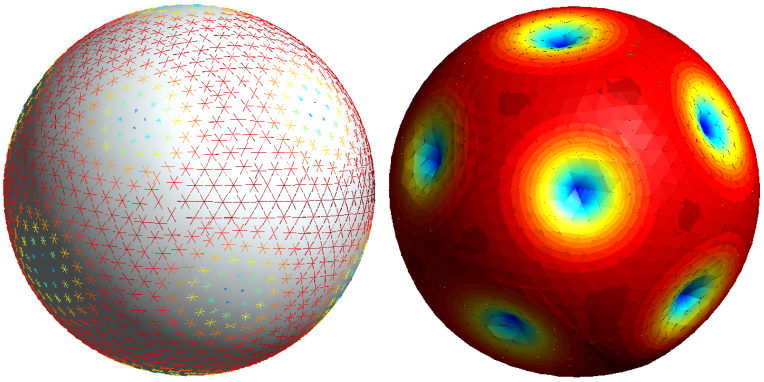

Figure 10: Cross field with 6 turns with their critical points on the corners of an icosahedron.

6.2. World oceans and seas

As it has been said previously, direction fields are used to generate points which are adequate for quadrangles (from cross fields), either equilateral triangles (from asterisk fields). Here, we show meshes that are built from such direction fields, by using algorithm of [13]. Some oceans and seas (up to geometry resolution and mesh size) are meshed over the Earth with only quadrangles, Fig. 11.

Figure 11: Quadrangular mesh of oceans and seas, built from cross fields.

On Fig. 12, we give results of cross (Fig. 12a) and asterik (Fig. 12b) fields. Observe that it is a zoom onto center of Fig. 11. Colorbar gives norm of branches within direction fields. Branches which color tends to blue (and thus zero norm) fairly correspond to critical points. We notice that critical points lay near boundaries (i.e. coasts). It means that repulsion of critical points is stronger than repulsion of boundary in (18). In other words, critical points tend to be close to boundaries (if any). There are more critical points within asterisk fields, than within cross fields. It is due to the fact that a nonregular vertex in a triangular mesh has an index of $\frac{\pm 1}{6}$, while in a quadrangular mesh it is $\frac{\pm 1}{4}$. Finally, we see that direction fields in both cases are smooth and enable production of high quality meshes with.

7. Conclusion

This article has mainly underlined the consistency of using Ginzburg-Landau equations to compute cross fields for indirect quadrangles meshing, and even so-called asterisk fields in order to produce equilateral triangles. The interest of using Ginzburg-Landau functional is related to its asymptotic behavior as the coherence length ϵ tends to zero: it gives optimal critical points of direction fields, i.e. those of lower index as it is expected by continuous and discrete topology. Besides, Ginzburg-Landau functional is intuitive with its two complementary terms: smoothing and penalty; it draws direction fields with aimed characteristics, as it has be shown by our results.

Acknowledgements

The present study was carried out in the framework of the project "Large Scale Simulation of Waves in Complex Media", which is funded by the Communauté Française de Belgique under contract ARC WAVES 15/19-03 with the aim of developing and using Gmsh [14].

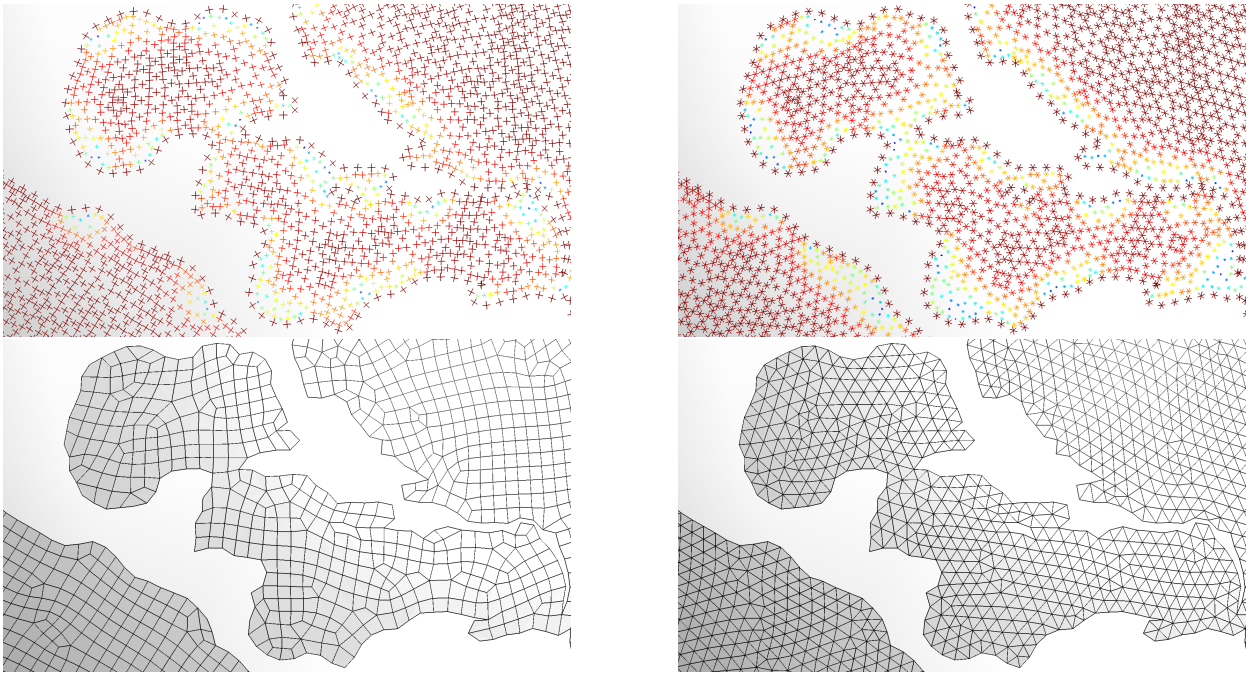

a. From cross fields.

b. From asterisk fields.

Figure 12: Output meshes from direction fields. Colorbar represents norm of direction branches.

References

[1] C. K. Lee, S. Lo, A new scheme for the generation of a graded quadrilateral mesh, Computers & structures 52 (1994) 847–857.

[2] J.-F. Remacle, J. Lambrechts, B. Seny, E. Marchandise, A. Johnen, C. Geuzaine, Blossom-Quad: A non-uniform quadrilateral mesh generator using a minimum-cost perfect-matching algorithm, International Journal for Numerical Methods in Engineering 89 (2012) 1102–1119.

[3] D. Bommes, H. Zimmer, L. Kobbelt, D. Bommes, H. Zimmer, L. Kobbelt, Mixed-integer quadrangulation, ACM Transactions on Graphics 28 (2009) 1.

[4] N. Kowalski, F. Ledoux, P. J. Frey, A PDE based approach to multidomain partitioning and quadrilateral meshing, Proceedings of the 21st International Meshing Roundtable, IMR 2012 (2013) 137–154.

[5] D. Eppstein, Nineteen proofs of euler's formula: $v - e + f = 2$, Information and Computer Sciences, University of California, Irvine (2009).

[6] N. Ray, B. Vallet, W. C. Li, B. Lévy, N-symmetry direction field design, ACM Transactions on Graphics 27 (2008) 1–13.

[7] F. Bethuel, H. Brezis, F. Hélein, Ginzburg-Landau Vortices, volume 13, Springer Science & Business Media, 2012.

[8] M. Crouzeix, P.-A. Raviart, Conforming and nonconforming finite element methods for solving the stationary stokes equations i, Revue française d'automatique, informatique, recherche opérationnelle. Mathématique 7 (1973) 33–75.

[9] N. Ray, D. Sokolov, B. Lévy, Practical 3d frame field generation, ACM Transactions on Graphics (TOG) 35 (2016) 233.

[10] E. B. Saff, A. B. Kuijlaars, Distributing many points on a sphere, The mathematical intelligencer 19 (1997) 5–11.

[11] P. D. Dragnev, D. Legg, D. Townsend, On the separation of logarithmic points on the sphere, in: Approximation Theory X: Abstract and Classical Analysis, Vanderbilt University Press, Nashville, TN, 2002, pp. 137–144.

[12] M. Fekete, Über die verteilung der wurzeln bei gewissen algebraischen gleichungen mit ganzzahligen koeffizienten, Mathematische Zeitschrift 17 (1923) 228–249.

[13] C. Georgiadis, P.-A. Beaufort, J. Lambrechts, J.-F. Remacle, Mesh generation on the sphere using cross and asterisk fields (2017). Submitted.

[14] C. Geuzaine, J.-F. Remacle, Gmsh: A 3-D finite element mesh generator with built-in pre- and post-processing facilities, International Journal for Numerical Methods in Engineering 79 (2009) 1309–1331.